X-ray photoelectron diffraction study of thin Al_2O_3 films grown on Si(111) by molecular beam epitaxy

M. El Kazzi,[1] G. Grenet,[1] C. Merckling,[1,2] G. Saint-Girons,[1] C. Botella,[1] O. Marty,[3] and G. Hollinger[1]
[1]*Institut des Nanotechnologies de Lyon INL-UMR5270, CNRS, Ecole Centrale de Lyon, Université de Lyon, Ecully F-69134, France*
[2]*STMicroelectronics, 850 rue Jean Monnet, 38926 Crolles Cedex, France*
[3]*Institut des Nanotechnologies de Lyon INL-UMR5270, CNRS, Campus de la Doua, Université de Lyon, Villeurbanne F-69622, France*
(Received 24 November 2008; revised manuscript received 3 March 2009; published 14 May 2009)

The in-plane and out-of-plane crystallographic orientations of Al_2O_3 films grown by molecular beam epitaxy on Si(111) have been determined by combining x-ray photoelectron diffraction (XPD) with transmission electron microscopy (TEM). On the one hand, polar and azimuth XPD curves for Al $2p$, O $1s$, and Si $2p$ core levels (recorded on a 6-nm-thick film) clearly indicate that Al_2O_3 grows (111) oriented on Si(111) but with two in-plane orientations: a "direct" one, i.e., $[11\bar{2}]Al_2O_3//[11\bar{2}]Si(111)$ and a "mirror" one, i.e., $[\bar{1}\bar{1}2]Al_2O_3(111)//[11\bar{2}]Si(111)$. On the other hand, a close inspection of the $40\bar{4}$ Al_2O_3 TEM diffraction spots (recorded on a 2-nm-thick film) reveals that these two in-plane orientations are slightly rotated with respect to the Si(111) orientations. These two results are consistent with an oxygen plane as the interfacial plane between $Al_2O_3(111)$ and Si(111).

DOI: 10.1103/PhysRevB.79.195312 PACS number(s): 81.15.Hi, 61.05.js, 68.55.aj

I. INTRODUCTION

Because of their many promising applications in nanotechnology, growing well-crystallized thin oxide films on silicon is the subject of intense activity. For example, high-κ oxides are expected to replace Hf-based dielectrics as gate material in forthcoming complementary metal-oxide-semiconductor (CMOS) technologies.[1,2] To achieve this, oxide films must have both a high crystallographic quality and a clear-cut interface with respect to Si. Fulfilling these two criteria is a particularly challenging task for two reasons: first, oxide orientation with respect to the Si is determined by a complex interplay between chemical-bonding optimization and lattice-mismatch energy minimization due to the difference in crystalline structure between oxides and silicon; second, and even more critical, Si is highly reactive to oxygen.[3,4] Earlier studies have shown that the oxide and the Si lattices connect via the oxide O sublattice.[5] Actually, to engineer clear-cut interfaces between functional oxides and silicon, some buffer layers, such as SrO,[6–8] BaO,[9] or $SrTiO_3$,[10] have to be grown to prevent the oxygen from reacting with silicon, especially at high growth temperatures and/or oxygen pressures.[11] Among potential buffers, alumina is a particularly appealing one due to its thermodynamic stability at temperatures and oxygen pressures up to 850 °C and 10^{-5} Torr, respectively. In fact, x-ray photoelectron spectroscopy (XPS) measurements[12] have shown that growing alumina on Si by molecular beam epitaxy (MBE) produces clear-cut interfaces without any formation of silica or silicates. If combined with high-κ oxides, growing alumina buffer thus provides an interesting means of achieving small equivalent oxide thicknesses (EOT) in CMOS devices.[13] However, the interest of studying and controlling the growth of alumina on silicon goes far beyond CMOSs because alumina could also be part of complex oxide/semiconductor heterostructures. Growing it on silicon may open the way to the integration of high performance micro-optoelectronic functionalities on Si wafers.[14]

Several groups[15,16] have already shown that Al_2O_3 is (111) oriented on Si(111). Our own studies[17] have shown that Al_2O_3 adopts a spinel-like structure (γ-Al_2O_3) on Si(111) with an interface that matches two surface-unit cells of $Al_2O_3(111)$ with three surface-unit cells of Si(111). Such an interface produces an effective tensile lattice mismatch ϵ of 2.9% where ϵ equals $(a_{Si}-a_{Al_2O_3})/a_{Al_2O_3}$ with $a_{Si}=0.5431$ nm for Si and $a_{Al_2O_3}=0.784\,76$ nm for γ-Al_2O_3. However, MBE-grown $Al_2O_3(111)/Si(111)$ films are known not to be exempt from twins and mosaicity usually attributed to growth mechanisms and related relaxation phenomena.

The present study combines x-ray photoelectron diffraction (XPD) and transmission electron microscopy (TEM) to give new insights into the growth mechanisms of γ-Al_2O_3 on Si(111). As a derivative of XPS, XPD singles out a chemical element as the photoelectron emitter and gives the usual information about its chemical surroundings. As a diffraction technique, XPD reveals all the crystallographic directions of the nearest neighbors of this photoelectron emitter.[18–20] But because XPD is a very short-range probe of the local atomic arrangement around the photoelectron emitter, it has to be compared to a long-range probe such as TEM.

II. RESULTS

Alumina (6-nm- or 2-nm-thick) films were grown on Si(111) substrates in a Riber 2300 MBE reactor by electron gun evaporation of Al_2O_3 targets under molecular oxygen. The Al_2O_3 growth rate was controlled *in situ* using a mass spectrometer. Details about the growth procedure can be found in Refs. 12 and 17. After growth, the samples were transferred to an XPS/XPD photoemission system. This apparatus is a vacuum science workshop (VSW) chamber equipped with a focused unpolarized monochromatic x-ray source (Al Kα=1486.6 eV). The detector acceptance angle is around 3°, and the angle between the x-ray source direc-

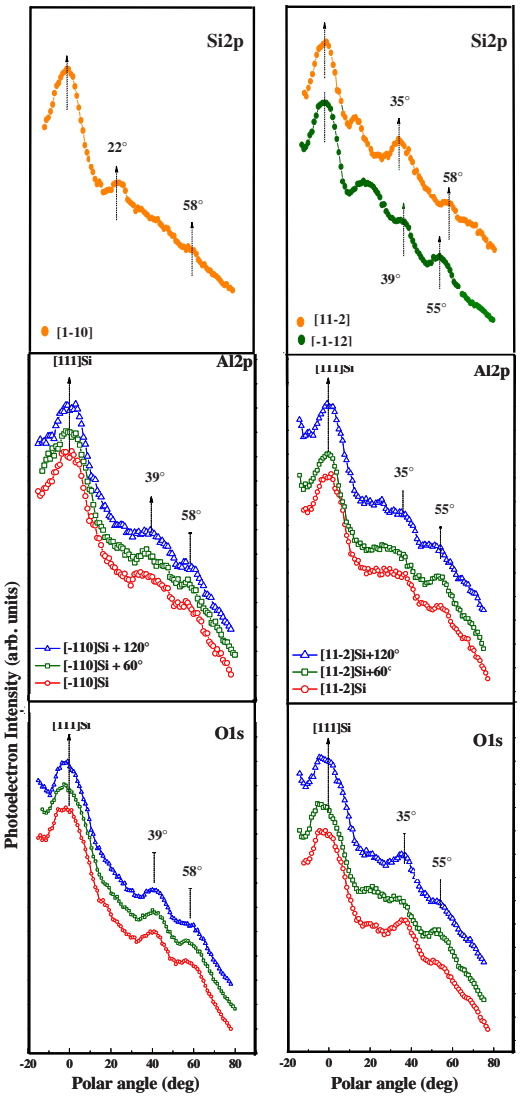

FIG. 1. (Color online) Si 2*p*, Al 2*p*, and O 1*s* photoelectron XPD polar curves recorded along the Si $\langle \bar{1}10 \rangle$ and $\langle 11\bar{2} \rangle$ azimuth directions for a bulk Si(111) substrate and a 6-nm-thick Al_2O_3 film grown on Si(111).

tion and the photoelectron detector direction is set at the "magic angle," i.e., 54.73°. During XPD curve recording, the sample is rotated step by step by motors with a precision better than 1°. According to both XPS and TEM, the interface between Al_2O_3 and Si is clear cut without any SiO_2 or silicates, and alumina is completely oxidized.[12]

A. XPD polar curves

Figure 1 shows polar curves for the Si 2*p* (kinetic energy=1386.6 eV), Al 2*p* (kinetic energy=1411 eV), and O 1*s* (kinetic energy=956 eV) photoelectrons recorded along the Si azimuth directions $\langle 1\bar{1}0 \rangle$ and $\langle 11\bar{2} \rangle$ for a bulk Si(111) substrate and an Al_2O_3 film grown on Si(111). The film was 6 nm thick. Even if Al and O have rather low atomic numbers and are thus rather poor diffusers, Al 2*p* and O 1*s* polar curves in Fig. 1 clearly show XPD features, i.e.,

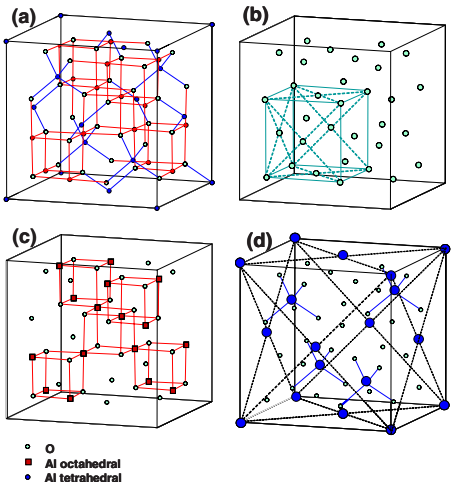

FIG. 2. (Color online) Tridimensional views of γ-Al_2O_3 unit cell: (a) all atoms and bondings; (b) the oxygen "face-centered" arrangement; (c) the octahedrally coordinated Al "rock-salt" lattice; and (d) the tetrahedrally coordinated Al lattice.

deviations from the usual monotonous intensity decreasing due to an increasing polar angle. These XPD features can be correlated with directions from a given emitter atom (either Al or O) site to one of its closest neighbors (Al or O) in Al_2O_3. We have chosen to index them on the basis of γ-Al_2O_3 crystallography.[21–23]

The γ-Al_2O_3 has a spinel structure (space group is $Fd\bar{3}m$) with enough Al vacancies to lead to the correct stoichiometry. The atomic locations in the γ-Al_2O_3 and Si unit cells are given in Table I for (001) and (111) crystal orientations. The coordinate system for (111) crystal orientation is

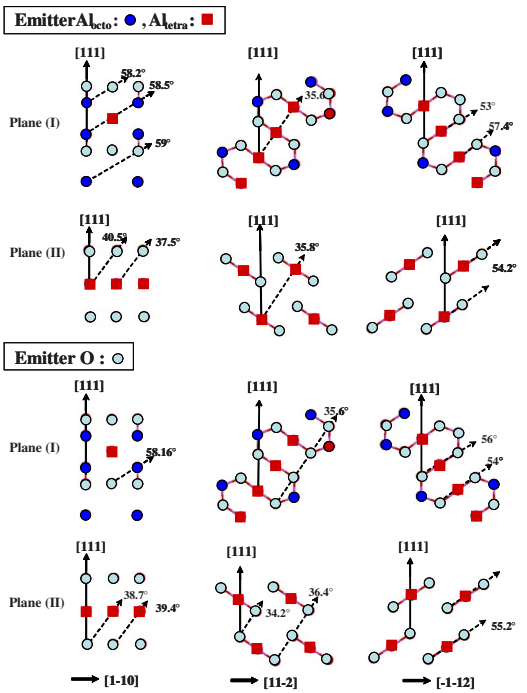

FIG. 3. (Color online) Two-dimensional views of the two kinds of γ-Al_2O_3 $\{1\bar{1}0\}$ and $\{11\bar{2}\}$ planes (labeled I and II).

TABLE I. Atomic positions $A_1 \ldots A_6$ for aluminum and $O_1 \ldots O_8$ for oxygen in the γ-Al_2O_3 lattice unit cell and atomic positions S_1, S_2 in silicon lattice unit cell. These coordinates are given for the two coordinate systems {[100],[010],[001]} for a (001) crystal orientation and {[11$\bar{2}$],[$\bar{1}$10],[111]} for a (111) crystal orientation. In this table, the distances are in lattice units (l.u.). For γ-Al_2O_3, the δ parameter equals to 0.004.

	(001)			(111)		
	[100]	[010]	[001]	[11$\bar{2}$]	[$\bar{1}$10]	[111]
			$\gamma-Al_2O_3$			
A_1	$\frac{1}{2}$	$\frac{1}{2}$	$\frac{1}{2}$	0	0	$\frac{\sqrt{3}}{2}$
A_2	$\frac{1}{2}$	$\frac{1}{4}$	$\frac{1}{4}$	$\frac{\sqrt{6}}{24}$	$-\frac{\sqrt{2}}{8}$	$\frac{\sqrt{3}}{3}$
A_3	$\frac{1}{4}$	$\frac{1}{2}$	$\frac{1}{4}$	$\frac{\sqrt{6}}{24}$	$\frac{\sqrt{2}}{8}$	$\frac{\sqrt{3}}{3}$
A_4	$\frac{1}{4}$	$\frac{1}{4}$	$\frac{1}{2}$	$-\frac{\sqrt{6}}{12}$	0	$\frac{\sqrt{3}}{3}$
A_5	$-\frac{1}{8}$	$-\frac{1}{8}$	$-\frac{1}{8}$	0	0	$-\frac{\sqrt{3}}{8}$
A_6	$\frac{1}{8}$	$\frac{1}{8}$	$\frac{1}{8}$	0	0	$\frac{\sqrt{3}}{8}$
O_1	$\frac{1+4\delta}{4}$	$\frac{1+4\delta}{4}$	$\frac{1+4\delta}{4}$	0	0	$\frac{\sqrt{3}(1+4\delta)}{4}$
O_2	$\frac{1+4\delta}{4}$	$-\delta$	$-\delta$	$\frac{\sqrt{6}(1+8\delta)}{24}$	$-\frac{\sqrt{2}(1+8\delta)}{8}$	$\frac{\sqrt{3}(1-4\delta)}{12}$
O_3	$-\delta$	$\frac{1+4\delta}{4}$	$-\delta$	$\frac{\sqrt{6}(1+8\delta)}{24}$	$\frac{\sqrt{2}(1+8\delta)}{8}$	$\frac{\sqrt{3}(1-4\delta)}{12}$
O_4	$-\delta$	$-\delta$	$\frac{1+4\delta}{4}$	$-\frac{\sqrt{6}(1+8\delta)}{12}$	0	$\frac{\sqrt{3}(1-4\delta)}{12}$
O_5	$-\frac{1+4\delta}{4}$	$+\delta$	$+\delta$	$-\frac{\sqrt{6}(1+8\delta)}{24}$	$\frac{\sqrt{2}(1+8\delta)}{8}$	$-\frac{\sqrt{3}(1-4\delta)}{12}$
O_6	$+\delta$	$-\frac{1+4\delta}{4}$	$+\delta$	$-\frac{\sqrt{6}(1+8\delta)}{24}$	$-\frac{\sqrt{2}(1+8\delta)}{8}$	$-\frac{\sqrt{3}(1-4\delta)}{12}$
O_7	$+\delta$	$+\delta$	$-\frac{1+4\delta}{4}$	$\frac{\sqrt{6}(1+8\delta)}{12}$	0	$-\frac{\sqrt{3}(1-4\delta)}{12}$
O_8	$-\frac{1+4\delta}{4}$	$-\frac{1+4\delta}{4}$	$-\frac{1+4\delta}{4}$	0	0	$-\frac{\sqrt{3}(1+4\delta)}{4}$
			Si			
S_1	$-\frac{1}{8}$	$-\frac{1}{8}$	$-\frac{1}{8}$	0	0	$-\frac{\sqrt{3}}{8}$
S_2	$\frac{1}{8}$	$\frac{1}{8}$	$\frac{1}{8}$	0	0	$\frac{\sqrt{3}}{8}$
			Lattice vectors			
a_1	0	$\frac{1}{2}$	$\frac{1}{2}$	$-\frac{\sqrt{6}}{12}$	$\frac{\sqrt{2}}{4}$	$\frac{\sqrt{3}}{3}$
a_2	$\frac{1}{2}$	0	$\frac{1}{2}$	$-\frac{\sqrt{6}}{12}$	$-\frac{\sqrt{2}}{4}$	$\frac{\sqrt{3}}{3}$
a_3	$\frac{1}{2}$	$\frac{1}{2}$	0	$\frac{\sqrt{6}}{6}$	0	$\frac{\sqrt{3}}{3}$

{[11$\bar{2}$],[$\bar{1}$10],[111]}. The γ-Al_2O_3 unit cell contains six nonequivalent aluminum sites (labeled A_1 to A_6 in Table I) and eight nonequivalent oxygen sites (labeled O_1 to O_8 in Table I) while the Si unit cell contains two nonequivalent silicon sites (labeled S_1 and S_2). Two-thirds of the Al cations (labeled A_1 to A_4) have octahedral coordination with oxygen while the last third (A_5 and A_6 in Table I) is tetrahedrally coordinated. The A_5 and A_6 coordinates in γ-Al_2O_3 are similar to the S_1 and S_2 ones in Si. Figure 2 shows an overall view of the spinel structure [Fig. 2(a)] along with three partial views. Figure 2(b) presents the face-centered-cubic (fcc) oxygen arrangement. Note that because the spinel structure contains vacancies as a regular part of the crystal, oxygen atoms are slightly shifted out of perfect fcc directions: in γ-Al_2O_3, shift δ equals 0.004. Figure 2(c) explains how the octahedrally coordinated Al and oxygen are arranged into a rock-salt lattice. Figure 2(d) singles out the tetrahedrally coordinated Al to make both their diamondlike organization and their tetrahedral bonding with oxygen explicit.

Figure 3 shows the atomic arrangement in the two kinds of γ-Al_2O_3 {1$\bar{1}$0} and {11$\bar{2}$} planes (labeled as I and II). In Fig. 3, atoms slightly out of the plane are represented because the shift parameter δ is too small to be of any importance when compared with the detector acceptance angle. The emitter-to-nearest-diffuser directions which are pertinent for this paper are collected in Tables II and III for the $\langle 11\bar{2} \rangle$ directions, i.e., $\phi=0$ or 180°, and the $\langle \bar{1}10 \rangle$ directions, i.e., $\phi=90$ or −90°, respectively. In these tables, polar angles θ are defined from the normal, i.e., the [111] axis, while azimuth angles ϕ are defined from the [11$\bar{2}$] axis.

Typically, in XPD curves, the normal at the surface is determined as the XPD maximum around $\theta=0°$. In the γ-Al_2O_3 case, though Al and O seem to be lined up with the [111] direction in Fig. 3, the experimental determination of

the normal at the surface is not as simple as usual because of the slight shift of the O atoms. In fact, a close inspection of the position and shape of the XPD maxima at $\theta=0°$ reveals some shifts and shoulders due to this bilateral asymmetry. In this respect, Table IV collects the emitter-to-nearest-diffuser directions around $\theta=0°$. The polar angle $\theta=0°$ was determined on the most bilaterally symmetrical polar curve, viz., Al $2p$ for $\phi=0°$ [Fig. 1 (left)].

In short, Al $2p$ and O $1s$ polar curves clearly exhibit XPD features around $\theta=0°$, $\theta=35°$, and $\theta=55°$ when the Si azimuth direction is $\langle 11\bar{2}\rangle$, and around $\theta=0°$, $\theta=39°$, and $\theta=58°$ when the Si azimuth direction is $\langle 1\bar{1}0\rangle$, in total agreement with Tables II and III. This denotes that Al_2O_3 has a structure which is very close to γ-Al_2O_3 oriented (111) when grown on Si(111). However, the polar curves for ϕ, $\phi+60°$, and $\phi+120°$ look very much alike though the [111] axis in γ-Al_2O_3 is a threefold axis. This apparent sixfold symmetry can be due to the coexistence of two alumina in-plane orientations, which can only be determined by recording XPD azimuth curves for some main polar angles.

B. XPD azimuth curves

The azimuth curves for Al $2p$ and O $1s$ recorded for polar angles $\theta=35°$ and $\theta=55°$ are reported in Fig. 4. For the sake of comparison, Fig. 4 also shows the same $\theta=35°$ and $\theta=55°$ XPD curves for Si $2p$ recorded on the Si(111) substrate. Figure 5 displays the positions of the diffuser atoms on cones with aperture of twice the polar angles $35\pm2.5°$ and $55\pm2.5°$, and with apex atoms Al, O, or Si for both γ-Al_2O_3 and Si(111). All the contributions from all the emitter sites have been added. In such a geometrical representation, the closer to the emitter or the heavier the diffuser, the higher the intensity in the corresponding XPD feature. In this regard, the forward scattering cross section for O $1s$ (Al $2p$) emitters is 11.4 (12.2) and 94.8 barns (100.6 barns) for O and Al diffusers, respectively.[24] In agreement with the literature,[25–27] Si $2p$ azimuth curves recorded for a Si(111) substrate exhibit a clear threefold symmetry with intense peaks every 120°, i.e., toward the Si $\langle 110\rangle$ directions ($\phi=0,120,240°$) for $\theta=35°$ and toward the Si $\langle 001\rangle$ directions ($\phi=60,180,300°$) for $\theta=55°$. According to Fig. 5, a threefold symmetry is also expected for the XPD azimuth curves of both the Al $2p$ and O $1s$ core levels in Al_2O_3 (111). In fact, the symmetry looks more sixfold than threefold because the main peaks are broader and the secondary peaks are more intense than the Si $2p$ ones in Si(111). Let us examine if this unexpected sixfold symmetry could be a consequence of Al being a heavier atom than O and thus a better diffuser. In others words, an Al atom acting as diffuser can give a greater XPD intensity than an O atom even if located farther from the emitter. According to Table II and Fig. 5, for Al $2p$ azimuth curves at $\theta=35°$ polar angle, the main XPD features are due to Al diffusers at 0.35 l.u. along the $\langle 110\rangle$ directions ($\phi=0,120,240°$) [Fig. 5(a)]. At 60° from these directions along the $\langle 114\rangle$ directions ($\phi=60,180,300°$) if XPD features are seen they are due to the same kind of diffusers (Al atoms) at 1.06 l.u. As the XPD intensity is proportional to the inverse square of the emitter-nearest-neighbor distance, the dif-

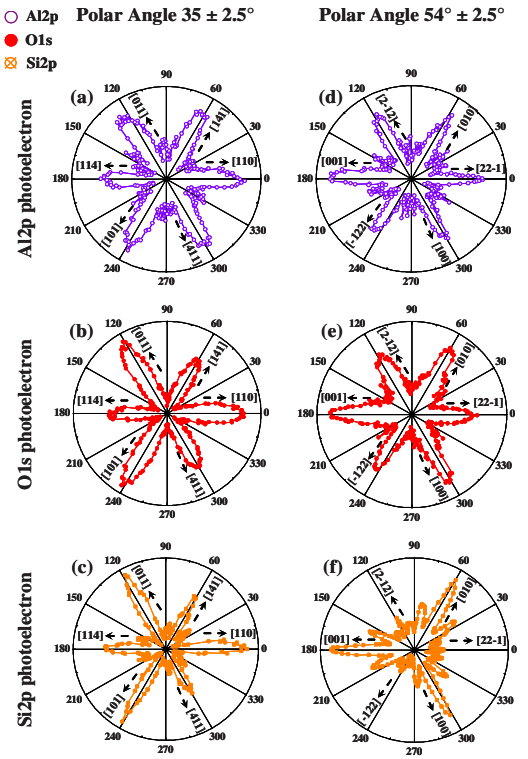

FIG. 4. (Color online) XPD azimuth curves of Al $2p$ and O $1s$ recorded on a 6 nm thick of Al_2O_3/Si(111) and of Si $2p$ recorded on Si(111) substrate for the 35 and 55° polar angles.

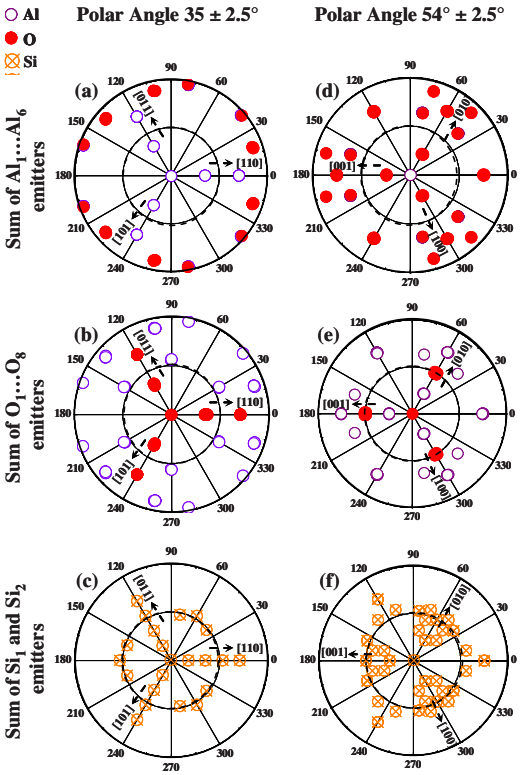

FIG. 5. (Color online) Diffuser locations (in l.u.) for polar angles $35\pm2.5°$ and $55\pm2.5°$ for all six Al (6) and eight O emitters in γ-Al_2O_3(111) and for the two Si emitters in Si(111). For Al_2O_3, the dashed circles correspond to 0.5 l.u. For Si, the dashed circles correspond to 2 l.u.

TABLE II. Emitter-to-nearest-diffuser directions and distances for γ−$Al_2O_3(111)$ $\langle 11-2\rangle$ directions, i.e., θ=0 or 180° and $\theta \leq 60°$. The distances are in l.u. The polar angle θ is from the normal, i.e., the [111] axis, while the azimuth angle ϕ is from the $[11\bar{2}]$ axis. Directions used for labeling XPD features have been highlighted in bold.

Al						Al						O						O					
E	D	θ	$\phi\approx0$	L		E	D	θ	$\phi\approx180$	L		E	D	θ	$\phi\approx0$	L		E	D	θ	$\phi\approx180$	L	
A_4	A_5	12.27	0.00	0.96	[553]	A_1	O_4	11.80	180.00	1.03	[223]	O_7	A_6	11.92	0.00	0.96	[553]	O_2	A_3	11.58	178.44	1.03	[223]
A_5	O_4	11.92	0.00	0.96	[553]	A_2	O_6	11.59	−178.44	1.03	[223]	O_1	A_4	15.94	0.00	0.74	[221]	O_3	A_2	11.58	−178.44	1.03	[223]
A_6	A_4	12.27	0.00	0.96	[553]	A_3	O_5	11.58	178.44	1.03	[223]	O_4	A_1	16.22	0.00	0.75	[221]	O_4	A_5	13.94	180.00	0.82	[223]
A_1	O_7	16.22	0.00	0.75	[221]	A_4	O_1	11.3	180.00	1.04	[223]	O_1	A_1	22.14	0.00	1.08	[331]	O_7	A_1	11.80	180.00	1.03	[223]
A_2	O_3	16.09	1.56	0.75	[221]	A_4	A_6	14.42	180.0	0.82	[335]	O_2	A_2	21.80	0.80	1.09	[331]	O_8	A_4	11.35	180.00	1.04	[223]
A_3	O_2	16.09	−1.56	0.75	[221]	A_5	A_4	14.42	180.00	0.82	[335]	O_3	A_3	21.80	−0.80	1.09	[331]	O_1	O_7	19.03	180.00	0.61	[112]
A_4	O_8	15.94	0.00	0.74	[221]	A_6	O_7	13.94	180.00	0.82	[335]	O_7	A_5	21.45	0.00	0.54	[331]	O_4	O_8	19.03	180.00	0.61	[112]
A_1	O_8	22.14	0.00	1.08	[331]	A_2	A_3	19.47	180.00	0.61	[112]	O_8	A_5	27.01	0.00	0.90	[551]	O_7	O_1	19.90	180.00	0.62	[112]
A_2	O_5	21.80	0.80	1.09	[331]	A_3	A_2	19.47	−180.00	0.61	[112]	**O_1**	**O_4**	**35.26**	**0.00**	**0.34**	**[110]**	O_8	O_4	19.90	180.00	0.62	[112]
A_3	O_6	21.80	−0.80	1.09	[331]	A_5	O_8	23.67	180.00	1.02	[337]	**O_2**	**O_6**	**33.97**	**0.00**	**0.35**	**[110]**	O_1	A_6	23.67	180.00	1.02	[337]
A_4	O_7	22.27	0.00	1.09	[331]	A_1	O_1	29.26	180.00	0.84	[113]	**O_3**	**O_5**	**33.97**	**0.00**	**0.35**	**[110]**	O_5	A_2	29.38	−179.20	0.83	[113]
A_5	A_6	22.00	0.00	1.09	[331]	A_2	O_2	29.38	−179.20	0.83	[113]	**O_4**	**O_1**	**35.26**	**0.00**	**0.37**	**[110]**	O_6	A_3	29.38	179.20	0.83	[113]
A_6	O_4	21.45	0.00	0.54	[331]	A_3	O_3	29.38	179.20	0.83	[113]	**O_5**	**O_3**	**36.56**	**0.00**	**0.35**	**[110]**	O_7	A_6	30.44	180.00	0.42	[113]
A_6	O_1	27.01	0.00	0.90	[551]	A_4	A_5	29.50	180.00	0.41	[113]	**O_6**	**O_2**	**36.56**	**0.00**	**0.35**	**[110]**	O_8	A_1	29.26	180.00	0.84	[113]
A_1	**A_4**	**35.26**	**0.00**	**0.35**	**[110]**	A_5	O_4	30.44	180.00	0.42	[113]	**O_7**	**O_8**	**35.26**	**0.00**	**0.34**	**[110]**	**O_1**	**O_4**	**35.84**	**180.00**	**1.06**	**[114]**
A_2	**A_2**	**35.26**	**0.00**	**0.71**	**[110]**	A_6	A_4	29.50	180.00	0.41	[113]	**O_8**	**O_7**	**35.26**	**0.00**	**0.37**	**[110]**	**O_2**	**O_6**	**35.41**	**180.00**	**1.07**	**[114]**
A_3	**A_3**	**35.26**	**0.00**	**0.71**	**[110]**	**A_1**	**A_4**	**35.26**	**180.00**	**1.06**	[114]	O_4	A_6	43.52	0.00	0.90	[55$\bar{1}$]	**O_3**	**O_5**	**35.41**	**180.00**	**1.07**	**[114]**
A_4	**A_1**	**35.26**	**0.00**	**0.35**	**[110]**	**A_4**	**A_1**	**35.26**	**180.00**	**1.06**	[114]	O_1	A_6	49.08	0.00	0.54	[33$\bar{1}$]	**O_4**	**O_1**	**34.69**	**180.00**	**1.07**	**[114]**
A_5	**A_5**	**35.26**	**0.00**	**0.71**	**[110]**	A_1	A_6	38.94	180.00	0.65	[115]	O_5	A_2	48.73	−0.40	1.09	[33$\bar{1}$]	**O_5**	**O_3**	**35.12**	**180.00**	**1.05**	**[114]**
A_6	**A_6**	**35.26**	**0.00**	**0.71**	**[110]**	A_5	A_1	38.94	180.00	0.65	[115]	O_6	A_3	48.73	0.40	1.09	[33$\bar{1}$]	**O_6**	**O_2**	**35.12**	**180.00**	**1.05**	**[114]**
A_5	O_7	43.52	0.00	0.90	[55$\bar{1}$]	A_6	O_8	39.33	180.00	0.64	[115]	O_7	A_4	48.39	0.00	1.08	[33$\bar{1}$]	**O_7**	**O_8**	**35.84**	**180.00**	**1.06**	**[114]**
A_1	O_1	48.26	0.00	1.09	[33$\bar{1}$]	A_5	O_7	42.91	180.00	0.89	[117]	**O_2**	**A_3**	**54.45**	**0.53**	**0.75**	**[22$\bar{1}$]**	**O_8**	**O_7**	**34.69**	**180.00**	**1.07**	**[114]**
A_2	O_2	48.73	−0.40	1.09	[33$\bar{1}$]	**A_1**	**O_7**	**53.42**	**180.00**	**0.25**	**[001]**	**O_3**	**A_2**	**54.45**	**−0.53**	**0.75**	**[22$\bar{1}$]**	O_1	A_5	39.33	180.00	0.64	[115]
A_3	O_3	48.73	0.40	1.09	[33$\bar{1}$]	**A_2**	**O_3**	**54.75**	**178.39**	**0.25**	**[001]**	**O_7**	**A_1**	**54.59**	**0.00**	**0.74**	**[22$\bar{1}$]**	O_4	A_6	42.91	180.00	0.90	[117]
A_4	O_4	48.39	0.00	1.08	[33$\bar{1}$]	**A_3**	**O_2**	**54.75**	**178.39**	**0.25**	**[001]**	**O_8**	**A_4**	**54.31**	**0.00**	**0.75**	**[22$\bar{1}$]**	**O_1**	**A_4**	**56.05**	**180.00**	**0.25**	**[001]**
A_5	O_8	49.08	0.00	0.54	[33$\bar{1}$]	**A_4**	**O_8**	**56.05**	**180.00**	**0.25**	**[001]**	O_1	A_5	58.61	0.00	0.96	[55$\bar{3}$]	**O_2**	**O_5**	**54.75**	**178.44**	**0.51**	**[001]**
A_6	A_5	48.53	0.00	1.09	[33$\bar{1}$]	**A_5**	**A_5**	**54.74**	**180.00**	**1.00**	**[001]**							**O_3**	**O_6**	**54.75**	**−178.44**	**0.51**	**[001]**
A_1	**O_4**	**54.59**	**0.00**	**0.74**	**[22$\bar{1}$]**	**A_6**	**A_6**	**54.74**	**180.00**	**1.00**	**[001]**							**O_4**	**A_1**	**53.42**	**180.00**	**0.25**	**[001]**
A_2	**O_6**	**54.45**	**−0.53**	**0.75**	**[22$\bar{1}$]**													**O_5**	**A_3**	**54.75**	**−178.39**	**0.25**	**[001]**
A_3	**O_5**	**54.45**	**0.53**	**0.75**	**[22$\bar{1}$]**													**O_6**	**A_2**	**54.75**	**178.39**	**0.25**	**[001]**
A_4	**O_1**	**54.31**	**0.00**	**0.75**	**[22$\bar{1}$]**													**O_7**	**O_4**	**56.01**	**180.00**	**0.51**	**[001]**
A_1	A_6	58.25	0.00	0.96	[55$\bar{3}$]													O_8	O_1	53.46	180.00	0.51	[001]
A_5	A_1	58.25	0.00	0.96	[55$\bar{3}$]																		
A_6	O_8	58.61	0.00	0.96	[55$\bar{3}$]																		

TABLE III. Emitter-to-nearest-diffuser directions and distances for γ-$Al_2O_3(111)$ $\langle -110 \rangle$ directions, i.e., ϕ=90 or −90° and $\theta \leq 60°$. The distances are in l.u. The polar angle θ is from the normal, i.e., the [111] axis, while the azimuth angle ϕ is from the $[11\bar{2}]$ axis. Directions used for labeling XPD features have been highlighted in bold.

Al						Al						O						O					
E	*D*	θ	$\phi \approx 90$	*L*		*E*	*D*	θ	$\phi \approx -90$	*L*		*E*	*D*	θ	$\phi \approx 90$	*L*		*E*	*D*	θ	$\phi \approx 90$	*L*	
A_1	A_4	22.21	90.00	0.94	[132]	A_1	A_4	22.21	−90.00	0.94	[312]	O_1	O_4	22.43	91.06	0.93	[132]	O_1	O_4	22.43	−91.06	0.93	[312]
A_4	A_1	22.21	90.00	0.94	[132]	A_4	A_1	22.21	−90.00	0.94	[312]	O_2	O_6	22.11	91.06	0.94	[132]	O_2	O_6	22.11	−91.06	0.94	[312]
A_5	O_7	28.48	88.94	0.74	[153]	A_5	O_7	28.48	−88.94	0.74	[513]	O_3	O_5	22.11	91.06	0.94	[132]	O_3	O_5	22.11	−91.06	0.94	[312]
A_1	**O_4**	**39.39**	**91.06**	**0.56**	[021]	**A_1**	**O_4**	**39.39**	**−91.06**	**0.56**	[201]	O_4	O_1	22.00	88.94	0.94	[132]	O_4	O_1	22.00	−88.94	0.94	[312]
A_2	**O_6**	**38.63**	**90.54**	**0.56**	[021]	**A_2**	**O_6**	**39.53**	**−90.52**	**0.56**	[201]	O_5	O_3	22.32	88.94	0.93	[132]	O_5	O_3	22.32	−88.94	0.93	[312]
A_3	**O_5**	**39.53**	**90.52**	**0.56**	[021]	**A_3**	**O_5**	**38.63**	**−90.53**	**0.56**	[201]	O_6	O_2	22.32	88.94	0.93	[132]	O_6	O_2	22.32	−88.94	0.93	[312]
A_4	**O_1**	**38.79**	**90.00**	**0.56**	[021]	**A_4**	**O_1**	**38.79**	**−90.00**	**0.56**	[201]	O_7	O_8	22.43	91.06	0.93	[132]	O_7	O_8	22.43	−91.06	0.93	[312]
A_1	A_5	47.43	90.00	0.96	$[\bar{1}73]$	A_1	A_5	47.43	−90.00	0.96	$[7\bar{1}3]$	O_8	O_7	22.00	88.94	0.94	[132]	O_8	O_7	22.00	−88.94	0.94	[312]
A_5	O_1	47.13	90.00	0.96	$[\bar{1}73]$	A_5	O_1	47.13	−90.00	0.97	$[7\bar{1}3]$	O_4	A_6	28.48	88.94	0.74	[153]	O_4	A_6	28.48	−88.94	0.74	[513]
A_6	A_1	47.43	90.00	0.96	$[\bar{1}73]$	A_6	A_1	47.43	−90.00	0.96	$[7\bar{1}3]$	**O_2**	**A_3**	**39.53**	**90.52**	**0.56**	**[021]**	**O_2**	**A_3**	**38.63**	**−90.54**	**0.56**	**[201]**
A_1	**O_8**	**58.93**	**90.00**	**0.83**	**$[\bar{1}31]$**	**A_1**	**O_8**	**58.93**	**−90.00**	**0.83**	**$[3\bar{1}1]$**	**O_3**	**A_2**	**38.63**	**90.54**	**0.56**	**[021]**	**O_3**	**A_2**	**39.53**	**−90.52**	**0.56**	**[201]**
A_2	**O_5**	**58.59**	**90.26**	**0.84**	**$[\bar{1}31]$**	**A_2**	**O_5**	**58.18**	**−90.27**	**0.83**	**$[3\bar{1}1]$**	**O_7**	**A_1**	**39.39**	**91.06**	**0.56**	**[021]**	**O_7**	**A_1**	**39.39**	**−91.06**	**0.57**	**[201]**
A_3	**O_6**	**58.18**	**90.27**	**0.83**	**$[\bar{1}31]$**	**A_3**	**O_6**	**58.59**	**−90.26**	**0.84**	**$[3\bar{1}1]$**	**O_8**	**A_4**	**38.79**	**90.00**	**0.56**	**[021]**	**O_8**	**A_4**	**38.79**	**−90.00**	**0.56**	**[201]**
A_4	**A_6**	**58.52**	**90.00**	**0.41**	**$[\bar{1}31]$**	**A_4**	**A_6**	**58.52**	**−90.00**	**0.42**	**$[3\bar{1}1]$**	O_8	A_6	47.13	90.00	0.97	$[\bar{1}73]$	O_8	A_6	47.13	−90.00	0.97	$[7\bar{1}3]$
A_5	**A_4**	**58.52**	**90.00**	**0.41**	**$[\bar{1}31]$**	**A_5**	**A_4**	**58.52**	**−90.00**	**0.42**	**$[3\bar{1}1]$**	**O_1**	**A_1**	**58.93**	**90.00**	**0.83**	**$[\bar{1}31]$**	**O_1**	**A_1**	**58.93**	**−90.00**	**0.83**	**$[3\bar{1}1]$**
A_6	**O_7**	**58.25**	**88.94**	**0.4**	**$[\bar{1}31]$**	**A_6**	**O_7**	**58.25**	**−88.94**	**0.42**	**$[3\bar{1}1]$**	**O_2**	**A_2**	**58.59**	**90.26**	**0.84**	**$[\bar{1}31]$**	**O_2**	**A_2**	**58.18**	**−90.27**	**0.83**	**$[3\bar{1}1]$**
												O_3	**A_3**	**58.18**	**90.27**	**0.83**	**$[\bar{1}31]$**	**O_3**	**A_3**	**58.59**	**−90.26**	**0.84**	**$[3\bar{1}1]$**
												O_4	**A_5**	**58.25**	**88.94**	**0.42**	**$[\bar{1}31]$**	**O_4**	**A_5**	**58.25**	**−88.94**	**0.42**	**$[3\bar{1}1]$**

TABLE IV. Table III: emitter-to-nearest-diffuser directions for γ-Al_2O_3 around the normal, viz., [111]. The distances are in l.u. As in Tables II and III, the polar angle θ is from the normal, i.e., the [111] axis, while the azimuth angle ϕ is from the $[11\bar{2}]$ axis.

Al				
E	D	θ	ϕ	L
A_1	O_8	0.0000	0.0000	0.4261
A_2	O_5	0.8597	120.0000	0.4354
A_3	O_6	0.8597	−120.0000	0.4354
A_4	O_7	0.8597	0.0000	0.4354
A_5	A_6	0.0000	0.0000	0.4330
A_6	O_1	0.0000	0.0000	0.2234
O				
E	D	θ	ϕ	L
O_1	A_1	0.0000	0.0000	0.4261
O_2	A_2	0.8597	120.0000	0.4354
O_3	A_3	0.8597	−120.0000	0.4354
O_4	A_4	0.8597	0.0000	0.4354
O_5	O_2	0.8689	−60.0000	0.8615
O_6	O_3	0.8689	60.0000	0.8615
O_7	O_4	0.8689	180.0000	0.8615
O_8	A_5	0.0000	0.0000	0.2234

ference in distance is large enough to make a clear difference to the XPD intensity. The same is true to some extent for Al $2p$ azimuth curves at the θ=55° polar angle for which the nearest diffusers are O atoms at 0.25 l.u. along the ⟨100⟩ directions (ϕ=60,180,300°) [Fig. 5(d)]. Other O diffusers exist along the $\langle 22\bar{1}\rangle$ directions (ϕ=0,120,240°) but far away at 0.75 l.u. Turning now to O 1s azimuth curves, at the θ=35° polar angle, the main XPD peaks are theoretically due to the O diffusers at 0.35 l.u. along the ⟨110⟩ directions (ϕ=0,120,240°) [Fig. 5(b)] and the secondary ones along the ⟨114⟩ directions (ϕ=60,180,300°) to the O diffusers at 1.07 l.u. Similarly, at the θ=55° polar angle, the diffusers are Al atoms at 0.25 l.u. along the ⟨100⟩ directions (ϕ=60,180,300°) [Fig. 5(e)] for the main XPD peaks and also Al atoms at 0.75 l.u. along the $\langle 22\bar{1}\rangle$ directions (ϕ=0,120,240°) for the secondary XPD peaks. In short, in every case considered, the main and secondary XPD peaks are produced by diffraction on the same chemical element, and the difference in emitter-diffuser distance is sufficient to produce a clear variation in XPD intensity. Therefore, we conclude that the observed sixfold symmetry is more probably explained by the existence of two domains labeled Δ1 and Δ2 of Al_2O_3 (111) rotated by 180° to each other: Δ1 with a direct relationship with the substrate, i.e., $[11\bar{2}]Al_2O_3$ (111)//$[11\bar{2}]$Si(111), and Δ2 with a mirror relationship, i.e., $[\bar{1}\bar{1}2]Al_2O_3$ (111)//$[11\bar{2}]$Si(111). This bidomain growth can be explained by the bonding between Al_2O_3(111) and Si(111) via an O plane. On the one hand, any plane of

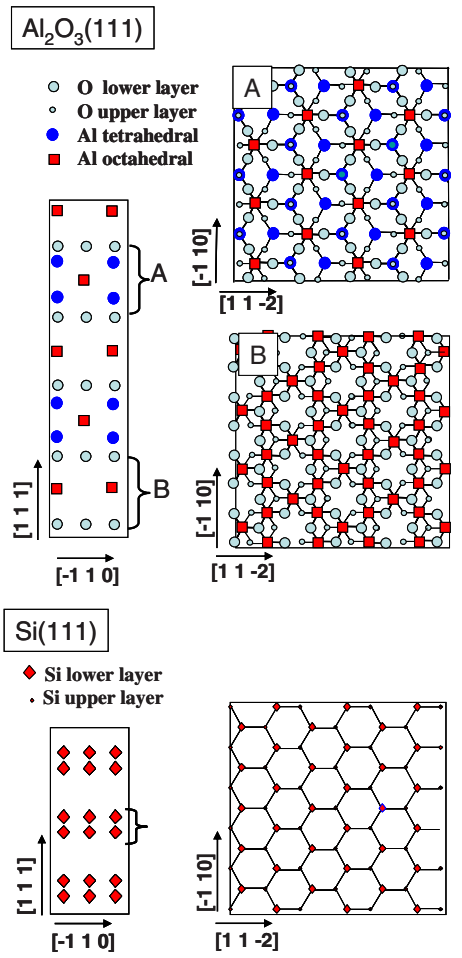

FIG. 6. (Color online) Al_2O_3(111) and Si(111) plane stacking. For Al_2O_3(111), the stacking is split into two parts for the sake of simplicity: one concerns the mixed tetragonal/octahedral Al plane; the other the octahedral Al plane.

Si(111) exhibits a sixfold symmetry. It is the sequence and the bonding of the Si planes along the [111] direction which give Si—and therefore the XPD diffraction—its unique threefold symmetry. On the other hand, the oxygen planes in Al_2O_3—in fact doublets—are also hexagonal in pattern. Here again, it is the plane stacking and bonding in Al_2O_3 that determines its orientation. This plane stacking and bonding is shown in Fig. 6 for Si(111) and γ-Al_2O_3(111). Moreover the Al_2O_3 plane stacking is itself made up, alternately, of the plane sequences labeled A or B in Fig. 6. Therefore, starting with a hexagonal O plane matching a hexagonal Si plane, the Al_2O_3 stacking process can proceed either as "direct" or "mirror," either "A" or "B." There is no reason for a preference which would in fact imply a fourth-neighbor plane interaction.

C. Cross-section transmission electron microscopy diffraction pattern

Figure 7 shows the in-plane electron diffraction pattern for a 2-nm-thick Al_2O_3 film on Si(111). The camera magnification, and thus the diffraction pattern scale, is determined

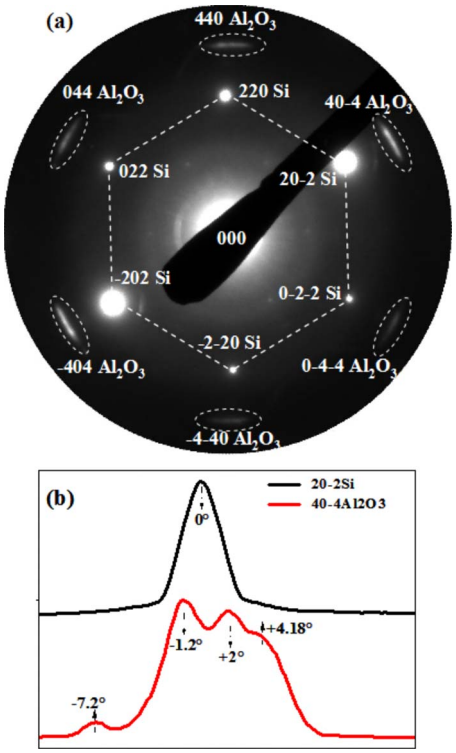

FIG. 7. (Color online) (a) In-plane electron diffraction pattern for a 2-nm-thick Al_2O_3 film on Si(111). (b) Contrast lines across $20\bar{2}$ Si and $40\bar{4}$ Al_2O_3 diffraction spots.

from the easily identified 220 Si bright spots. The other diffraction spots are ascribed to the Al_2O_3 film. They correspond to an interplane distance of 0.1396 ± 0.0007 nm, a value close to the {440} interplane distance of γ-Al_2O_3, viz., $d_{440}=0.1399 \pm 0.0004$ nm in Refs. 28 and 29. Therefore, in agreement with the XPD observations, the {440} Al_2O_3 planes are found to be parallel to the {220} Si planes. Let us compare the contrast profile of the $20\bar{2}$ Si spot and that of $40\bar{4}$ Al_2O_3 shown in Fig. 7(b). The extension of the $40\bar{4}$ Al_2O_3 diffraction spot is much larger than that of the $20\bar{2}$ Si diffraction spot. This expansion is structured into three features with maxima at −1.2, +2, and 4.18° from the $20\bar{2}$ Si diffraction spot. This implies that some {110} Al_2O_3 planes are both turned away from one another and therefore from the {110} Si planes. This result is not surprising as oxygen atoms are naturally slightly shifted in cubic γ-Al_2O_3 (Table I). These shifts induce a tilt in the ⟨110⟩ direction normally at $\theta=35.26°$ to either $\theta=33.97$ or 36.56° (Table II). Also, the tensile stress imposed by the Si(111) substrate on the Al_2O_3 thin film can also slightly shift the O locations toward higher polar angles.

III. CONCLUSION

In this work, we have combined XPD with TEM to study the growth of Al_2O_3 on Si(111). The well-defined XPD features in the polar and azimuth curves recorded for Al 2*p*, O 1*s*, and Si 2*p* core levels have all been ascribed to spinel γ-Al_2O_3 crystallographic directions, a fact that clearly reflects that the alumina films grown by MBE are of high crystallographic quality. Our XPD results indicate unambiguously that Al_2O_3 grows (111) oriented with two in-plane orientations: a direct one, i.e., $[11\bar{2}]Al_2O_3$ (111)//$[11\bar{2}]$Si(111), and a mirror one, i.e., $[\bar{1}\bar{1}2]Al_2O_3$ (111)//$[11\bar{2}]$Si(111). These two orientations result from the intrinsic pattern and sequence of Al_2O_3 planes in the ⟨111⟩ growth direction. Therefore, making one of them prevail is certainly a very demanding task. However, such intrinsic mosaicity is probably not damaging for a number of applications.

ACKNOWLEDGMENTS

The authors would like to thank P. Regreny for helpful discussions and J. B. Goure for technical assistance.

[1] D. G. Wilk, R. M. Wallace, and J. M. Anthony, J. Appl. Phys. **89**, 5243 (2001).
[2] J.-P. Locquet, C. Marchiori, M. Sousa, J. Fompeyrine, and J. W. Seo, J. Appl. Phys. **100**, 051610 (2006).
[3] K. J. Hubbard and D. G. Schlom, J. Mater. Res. **11**, 2757 (1996).
[4] D. G. Schlom and J. H. Haeni, MRS Bull. **27**, 198 (2002).
[5] A. Fissel, H. J. Osten, and E. Bugiel, J. Vac. Sci. Technol. B **21**, 1765 (2003).
[6] X. Hu, H. Li, Y. Liang, Y. Yu, D. Marshall, J. Edwards, Jr., R. Droopad, X. Zhang, A. A. Demkov, and K. Moore, Appl. Phys. Lett. **82**, 203 (2003).
[7] G. Delhaye, C. Merckling, M. El-Kazzi, G. Saint-Girons, M. Gendry, Y. Robach, G. Hollinger, L. Largeau, and G. Patriarche, J. Appl. Phys. **100**, 124109 (2006).
[8] M. El Kazzi, G. Delhaye, C. Merckling, E. Bergignat, Y. Robach, G. Grenet, and G. Hollinger, J. Vac. Sci. Technol. A **25**, 1505 (2007).
[9] R. A. McKee, F. J. Walker, J. R. Conner, E. D. Specht, and D. E. Zelmon, Appl. Phys. Lett. **59**, 782 (1991).
[10] C. Merckling, G. Delhaye, M. El-Kazzi, S. Gaillard, Y. Rozier, L. Rapenne, B. Chenevier, O. Marty, G. Saint-Girons, M. Gendry, Y. Robach, and G. Hollinger, Microelectron. Reliab. **47**, 540 (2007).
[11] C. Merckling, M. El-Kazzi, L. Beccera, L. Largeau, G. Patriarche, G. Saint-Girons, and G. Hollinger, Microelectron. Eng. **84**, 2243 (2007).
[12] C. Merckling, M. El-Kazzi, V. Favre-Nicolin, M. Gendry, Y. Robach, G. Grenet, and G. Hollinger, Thin Solid Films **515**, 6479 (2007).
[13] L. Becerra, C. Merckling, N. Baboux, M. El-Kazzi, G. Saint-Girons, B. Vilquin, C. Plossu, and G. Hollinger, in *Materials Science of High-k Dielectric Stacks—From Fundamentals to Technology*, edited by L. Pantisano *et al.*, MRS Symposia Proceedings No. 1073E (Materials Research Society, Warrendale,

PA, 2008).
[14] G. Saint-Girons, P. Regreny, L. Largeau, G. Patriarche, and G. Hollinger, Appl. Phys. Lett. **91**, 241912 (2007).
[15] T. Okada, M. Ito, K. Sawada, and M. Ishida, J. Cryst. Growth **290**, 91 (2006).
[16] S. Y. Wu, M. Hong, A. R. Kortan, J. Kwo, J. P. Mannaerts, W. C. Lee, and Y. L. Huang, Appl. Phys. Lett. **87**, 091908 (2005).
[17] C. Merckling, M. El-Kazzi, G. Saint-Girons, G. Hollinger, L. Largeau, G. Patriarche, V. Favre-Nicolin, and O. Marty, J. Appl. Phys. **102**, 024101 (2007).
[18] C. S. Fadley, in *Synchrotron Radiation Research, Advances in Surface*, edited by R. Z. Bachrach (Plenum, New York, 1990).
[19] S. A. Chambers, Adv. Phys. **40**, 357 (1991).
[20] G. Grenet, Y. Jugnet, S. Homberg, H. C. Poon, and Tran Minh Duc, Surf. Interface Anal. **14**, 367 (1989).
[21] H. P. Pinto, R. M. Nieminen, and S. D. Elliott, Phys. Rev. B **70**, 125402 (2004).
[22] E. Menéndez-Proupin and G. Gutiérrez, Phys. Rev. B **72**, 035116 (2005).
[23] P. Boulenc and I. Devos, Mater. Sci. Semicond. Process. **9**, 949 (2006).
[24] NIST Electron Elastic-Scattering Cross-Section Database.
[25] S. Van, D. Steinmetz, D. Bolmont, and J. J. Koulmann, Phys. Rev. B **50**, 4424 (1994).
[26] L. Simon, D. Aubel, L. Kubler, J. L. Bischoff, J. Gewinner, and J. L. Balladore, J. Appl. Phys. **81**, 2635 (1997).
[27] S. Bengió, M. Martin, J. Avila, M. C. Asensio, and H. Ascolani, Phys. Rev. B **65**, 205326 (2002).
[28] ICDD database, PDF No. 00–010–0425.
[29] ICDD database, PDF No. 00–050–0741.